Materials Science in Semiconductor Processing 40 (2015) 890–895

Contents lists available at ScienceDirect

Materials Science in Semiconductor Processing

journal homepage: www.elsevier.com/locate/mssp

Tin oxide based dye-sensitized solid-state solar cells: surface passivation for suppression of recombination

C.S.K. Ranasinghe [a,b], E.N. Jayaweera [a,b], G.R.A. Kumara [b,*], R.M.G. Rajapakse [a,b], B. Onwona-Agyeman [c], A.G.U. Perera [d], K. Tennakone [d]

[a] Postgraduate Institute of Science, University of Peradeniya, Peradeniya 20400, Sri Lanka
[b] Department of Chemistry, Faculty of Science, University of Peradeniya, 20400, Sri Lanka
[c] Department of Materials Science and Engineering, University of Ghana, Ghana
[d] Department of Physics and Astronomy, Georgia State University, Atlanta, United States

ARTICLE INFO

Article history:
Received 2 February 2015
Received in revised form
16 July 2015
Accepted 16 July 2015
Available online 7 August 2015

Keywords:
Dye-sensitized solid-state solar cell
Surface passivation
Recombination suppression
Indoline D149
Tin(IV) oxide
Magnesium oxide

ABSTRACT

Dye-sensitized solid-state solar cells based on SnO_2 where the crystallite surface is passivated with ultra-thin structures constituted of MgO, ZnO and CaO are examined using high extinction coefficient indoline dye D149 as the sensitizer. Results clearly demonstrate that surface passivation effectively suppress leakage of electrons from interconnected SnO_2 crystallites preventing recombination with the hole transport substrate CuSCN. In the presence of passivating films of any type, the optimum efficiency occurred at nearly same SnO_2 film thickness of 12 μm. MgO passivated system at a MgO surface concentration of $\sim 8 \times 10^{-9}$ g cm^{-2} yielded the highest efficiency of 2.82% under standard measurements conditions using cells of active area 0.25 cm^2.

1. Introduction

Solar cells based on heterojunctions of the configuration, nano-structured n-type semiconductor/thin light harvesting layer/p-type semiconductor has attracted great deal attention as a promising concept for the development solar cells, via less energy intensive and environmentally friendly techniques [1–12]. The light harvesting layer (LHL) could be a dye [1–5,10,12,13] (D) or a semiconductor (S) [6–11] with interfaces establishing electronic communication with the n- and p-type collector substrates. When LHL=D, the resulting device referred to as the dye-sensitized solid-state solar cell (DSSC), delivers a photocurrent, when the excited molecules D inject, electrons and holes to n- and p-substrates from the LUMO and HOMO levels [13]. Similarly, when LHL=S, the resulting device, named the extremely thin absorber solar cell [6–8] (ETA cell) operates by diffusive transfer of photo-generated electrons and holes in conduction and valence bands states (CB and VB) of S to the n- and p-substrates [6]. Although there are fundamental distinctions in the detailed mechanism of operation of DSSCs and ETA cells, the requisite material aspects of n- and p-type substrates are similar. The n-type material should essentially be an optically transparent stable semiconductor admitting deposition onto conducting transparent glass to form a thin film constituted of interconnected nano-crystallites. Again the film roughness factor needs to be of the order of one thousand, in order to obtain a sufficiently large light absorption cross-section on deposition of LHE. For efficient collection of electrons at the anode, the film thickness should not exceed the electron diffusion length [$L=(D\tau)^{1/2}$], (where D=diffusion coefficient, τ=recombination time) in the matrix and the necessary roughness factor is achieved by reducing the crystallite size and introducing porosity to the film. Porosity also leads to a significant population of interconnected void paths leading to the back contact. Unlike in the dye-sensitized electrolytic cell, in a DSSC or ETA cell, filling of these channels by the hole-collector, results short-circuiting of the cell. Elimination or minimization of void channels in the film is essential for proper functioning of a DSSC or an ETA cell. In the first reported DSSC [1] and the ETA cell [6], this requirement was achieved by an ingenious film fabrication procedure involving multiple application and sintering of a especially prepared TiO_2 paste on conducting tin oxide glass [1,6]. Later, a more convenient method of depositing a blocking layer and an upper screen printed layer was adopted [14].

A variety techniques have been developed for depositing nano-structured thin films of familiar high band oxide semiconductors TiO_2 [15], ZnO [7,16–18] and SnO_2 [19–22] and they have been

* Corresponding author.

http://dx.doi.org/10.1016/j.mssp.2015.07.042
1369-8001/

extensively examined as the n-type substrate for electrolytic dye-sensitized solar cells [7,16–22]. Of these highest unmatched efficiencies with best sensitizer dyes were achieved with TiO_2, despite the variation of the film morphology in the case of other two oxides. Cells based on ZnO and SnO_2 are highly susceptible to recombination owing to heavier population of surface states [16–22]. Although the mechanism involved has not been fully understood, it appears that, lower effective carrier mass in SnO_2 facilitates recombination mediated via surface states [19]. Surface modifications passivate surface the states and as expected, deposition of ultra-thin layers of insulating or semiconducting oxides impressively enhances the efficiencies of electrolytic dye-sensitized SnO_2 solar cells based cells [19]. Tin oxide has some advantages over TiO_2 because of higher diffusion rates of electrons in bulk SnO_2 [18,19]. Unfortunately, in nanocrystalline SnO_2 films, the diffusion coefficient happens to be even smaller than that of TiO_2 owing to presence surface traps, trapping–detrapping greatly reduce the effective diffusion coefficient. Closure of surface states, increases the effective diffusion coefficient of electrons in SnO_2 permitting the usage of thicker films to increase the light absorption cross-section. Attempts have also been made to utilize SnO_2 as n-type substrate for DSSCs, adopting the strategy of surface passivation [23–25]. Experiments with MgO passivating layers have clearly demonstrated that, it slows down recombination kinetics, but lowers the injection rate. In this work we describe our observation on SnO_2 based DSSCs, surface passivated with ultra-thin films of MgO, ZnO and CaO and sensitized with the high extinction coefficient organic indoline dye D149 [26]. The variation of the photovoltaic parameters with respect to the thickness of the composite film is examined in detail for MgO, ZnO and CaO.

2. Material and methods

In all experiments, sample solar cells were fabricated using fluorine doped tin oxide (FTO) glass plates (sheet resistance 20 Ω/sq and dimensions 1×2 cm^2) adopting the following procedure. The layer FTO in an area of thickness ~1 mm along three edges of the plate was ablated with Zn+HCl treatment after insertion of a mask. To deposit a blocking layer of un-doped SnO_2, the bare area along the edges is again masked, plate heated to 450 °C and a solution of dibutyltindiacetate (7.5% in ethanol) sprayed evenly. Pryolysis of tin precursor yields a transparent SnO_2 layer of sheet resistance ~0.1 k Ω/sq, when the extent of spraying is controlled accordingly. For the purpose establishing electrical contact, a patch of silver paste, ~0.25 cm wide is painted at the FTO covered edge of the plate. The steps of the above procedure are depicted in (a)–(c) of Fig. 1.

Mesoporous SnO_2 films were deposited on the plates processed as above using a 15% aqueous colloidal solution of SnO_2 (Alfar-Aesar). Three drops of glacial acetic acid is added to 2 ml of the colloidal solution and the mixture is ground in an agate mortar to

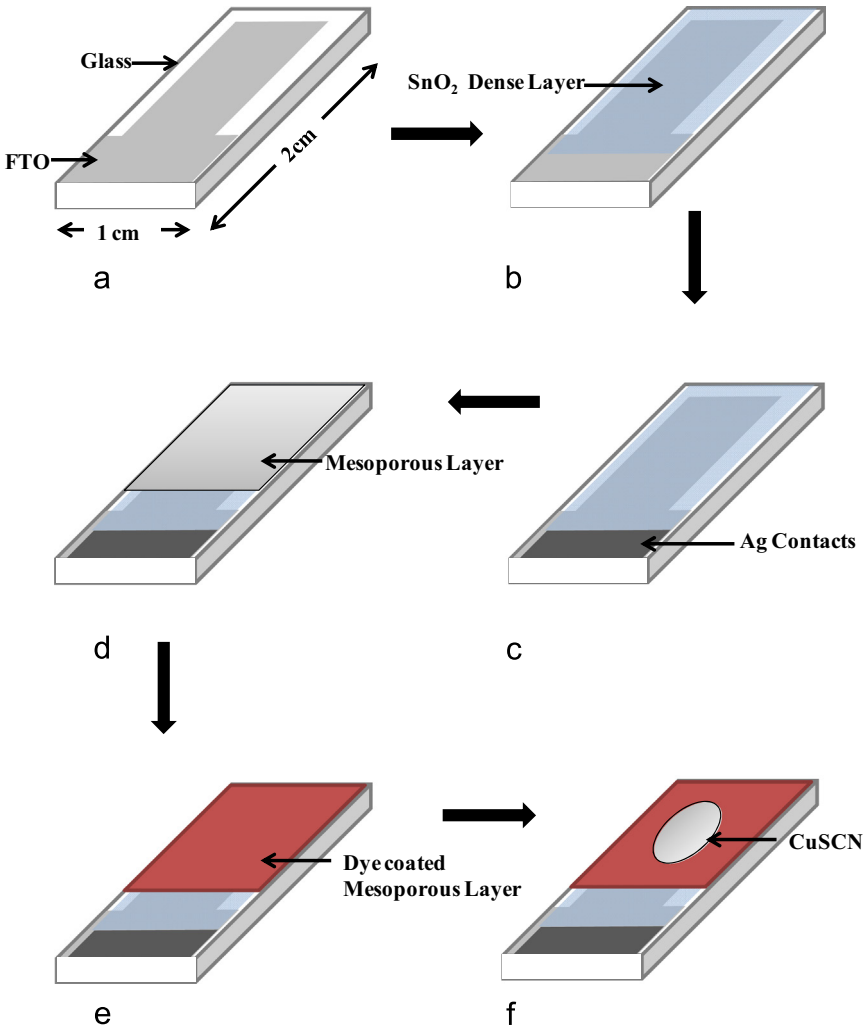

Fig. 1. (a) Removing FTO at the edges, (b) application of SnO_2 blocking layer, (c) deposition of Ag contact, (d) deposition of SnO_2 based mesoporous film, (e) dye coating of the mesoporous film, and (f) deposition of CuSCN.

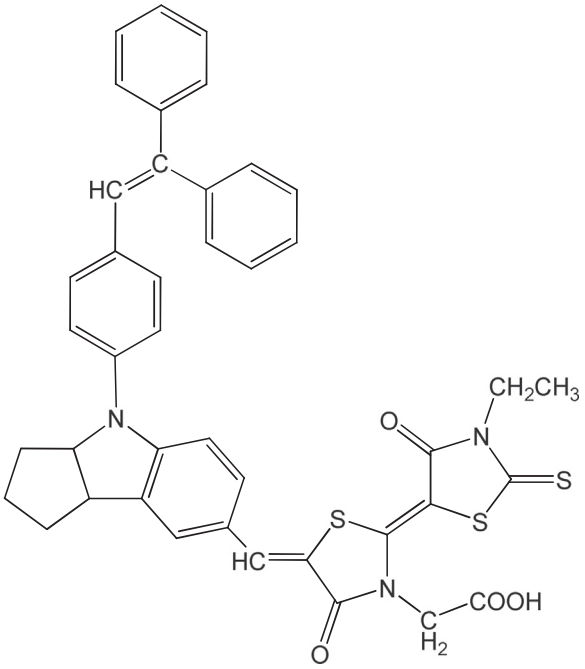

Fig. 2. Structure of the D149 dye.

form a thick paste and ground again after addition of 3 ml of the non-ionic surfactant Triton X 100. The paste was dispersed in 40 ml ethanol and sprayed on the plate heated to 150° C, appropriately masked to expose only the blocking layer area. Finally the plate is heated in air at 500 °C for 30 min to form the SnO_2 film [Fig. 1(c)]. Composite films covered with ultra-thin barrier layers over SnO_2 crystallites were prepared by incorporation weighed quantities of MgO, ZnO and $CaCO_3$ into the SnO_2+acetic acid mixture prior to grinding. Films were characterized by SEM and XRD. SEM images of transverse sections of plates were recorded to determine the films thickness.

The dye used in all the experiments is the indoline D149 whose structural formula is given in Fig. 2. The dye is coated by immersing the plates in a solution of the 0.3 mM solution of dye (acetonitrile+t-butanol in 1:1 ratio by vol.) for 12 h. Plates are rinsed with acetonitrile, dried and stored in dark.

CuSCN was deposited on the dyed area of the plates by a modification of the procedure previously adopted [27] to improve the film morphology and enhance p-type conductivity of CuSCN. Pure CuSCN (0.5 g) is dissolved in n-propyl sulfide and ~1 ml triethylaminethiocyanate is mixed and agitated in air for about a minute. Thereafter the solution is aged for about a week in a closed vial and any brown precipitate settling down is removed by decantation [28]. Solution is drop coated over dyed plate heated to 80 °C and slowly dried to the ambient. The above prescription for coating CuSCN, effectively introduce excess SCN to CuSCN enhancing p-type conductivity [28], traces of SCN^- ions in the solvent acts as a crystal growth inhibitor aiding pore filling.

Cells set for measurements are fabricated by painting the outer CuSCN surface with graphite and pressing a Cr–Pt coated FTO glass plate to serve as the cathode. Here, the hole collector is CuSCN and graphite is used to improve the contact between Cr–Pt coated FTO glass and CuSCN layer. A cross-section of the cell depicting different components of heterojunction is presented in Fig. 3. The cells masked to an active area of 0.25 cm^2 were used to ascertain *IV* characteristics at AM1.5 simulated sunlight using Peccell L01 solar simulator and a source meter. The variation of *IV* parameters with film thickness and amount of passivating material (MgO, ZnO and CaO) was investigated to determine the optimum efficiency.

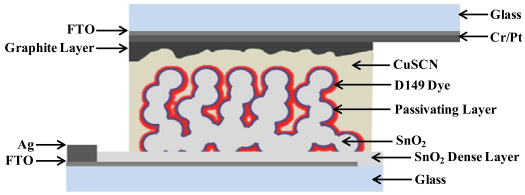

Fig. 3. Schematic sketch showing different components of the heterojunction.

The internal cell parameters were determined by impedance spectroscopy using Autolab PGSTAT12 system at dark conditions, at bias voltage of −0.5 V and in the frequency range from 1 mHz to 1 MHz.

3. Results and discussion

Tin oxide films made by the procedure described in the experimental section have a mesoporous structure (SEM) with crystallites of median size 3–5 nm and roughness factor of 500–600 determined by standard dye desorption technique. In cells made only of SnO_2 (i.e. no surface passivating agent included in the film fabrication procedure), the optimum of *IV* parameters (J_{sc}=6.07 mA cm^{-2}, V_{oc}=0.156 V, FF=0.334, η=0.32%) occurred when the film thickness is 9±1 μm (Table 1). When the thickness variation of *IV* parameters was examined in films incorporating the passivating agent, the optimum of η and I_{sc} occurred at a fixed level of loading of MgO, ZnO, CaO of $\sim 3.6\times10^{-3}$, 1.2×10^{-2}, and 6×10^{-2} g per 1 g of SnO_2 respectively. These optimum loadings in each case are largely independent of the film thickness.The above values corresponds to a surface coverage of MgO, ZnO, CaO on SnO_2 crystallites at concentrations $\sim 8\times10^{-9}$, 2.8×10^{-8}, and 1.4×10^{-8} g cm^{-2} respectively. A simple estimation assuming bulk densities of these oxides, indicates that film thickness *t* calculated as $t=w/A\rho$ (w=wt. of passivating material, A=effective area of the film, ρ=bulk density of the passivating material) is even less than the respective unit cell dimensions. Presumably, the passivating layer is a modified surface structure of sub-nanometer dimensions not resolved in XRD or SEM. Sometimes XRD examination of the films display peaks suggestive individual oxides, their stannates or carbonates. Perhaps, these signals originate from un-homogenized islets of the additive material accumulating in the film matrix.

Tables 2–4 show the film thickness variation of the *IV* parameters of the cells based on SnO_2/MgO, SnO_2/ZnO and SnO_2/CaO films at the optimum surface concentrations of MgO, ZnO and CaO. For all the three cases the optimum efficiencies of 2.82%, 2.38%, and 1.38% respectively corresponded to a film thickness of 12 μm, compared to 9 μm for the cells where the SnO_2 surface remained unmodified. This observation can be understood as effective mitigation of electrons injected to the semiconductor matrix, recombining with holes at the interface, during their transit to the back contact. Again passivation of the trapping sites reduces the frequency of trapping and detrapping events increasing the effective diffusion coefficient [29,30] $D_{eff}\sim n_c(n_c+n_t)$, where

Table 1
I–V parameters of cells with SnO_2 films of different thicknesses.

Cell no.	SnO_2 film thickness ± 1/ μm	J_{sc}/mA/cm^2	V_{oc}/V	FF	Efficiency/%
1	3	3.82	0.094	0.289	0.10
2	6	3.73	0.110	0.295	0.12
3	9	6.07	0.156	0.334	0.32
4	12	3.76	0.100	0.290	0.11
5	15	1.78	0.056	0.268	0.03

Table 2
IV parameters of SnO_2/MgO cells of different film thicknesses at the optimum surface concentration of MgO.

	SnO_2/MgO film thickness ± 1/ μm	J_{sc}/mA/cm^2	V_{oc}/V	FF	Efficiency/%
1	3	4.43	0.500	0.403	0.89
2	6	5.61	0.550	0.537	1.66
3	9	8.66	0.549	0.476	2.26
4	12	10.18	0.544	0.510	2.82
5	15	8.86	0.533	0.530	2.50

Table 3
IV parameters of SnO_2/ZnO cells of different film thicknesses at the optimum surface concentration of ZnO.

Cell no.	SnO_2/ZnO film thickness ± 1/μm	J_{sc}/mA/cm^2	V_{oc}/V	FF	Efficiency/%
1	3	3.47	0.556	0.529	1.02
2	6	8.25	0.503	0.370	1.54
3	9	8.85	0.489	0.388	1.68
4	12	10.24	0.507	0.459	2.38
5	15	8.26	0.474	0.444	1.74

Table 4
IV parameters of SnO_2/CaO cells of different film thicknesses at the optimum surface concentration of CaO.

Cell no.	SnO_2 film thickness ± 1/ μm	J_{sc}/mA/cm^2	V_{oc}/V	FF	Efficiency/%
1	3	3.60	0.412	0.414	0.61
2	6	7.84	0.442	0.426	1.48
3	9	7.95	0.448	0.458	1.63
4	12	8.84	0.454	0.458	1.84
5	15	6.24	0.364	0.384	0.87

n_c=density of free electrons, n_t=density of trapped electrons As recombination time τ and diffusion coefficient are both increased, the electron diffusion length $(D_{eff}\tau)^{1/2}$greatly increases and the film thickness is limited by mean free path of light. The dye D149 has a high extinction coefficient of the order of 70,000 L mol cm^{-1} near the absorption peak [31] corresponding to photon mean free path of the 10 μm in the dyed film.

Fig. 4 shows *IV* curves for the cells based on SnO_2/MgO, SnO_2/ZnO,SnO_2/CaO films at the optimum surface concentration of MgO, ZnO, and CaO respectively and for comparison the *IV* curve for the cells made of unmodified SnO_2.The highest efficiency (2.82%), open-circuit voltage (0.544 V) fill factor (0.510) is obtained in the MgO system. These parameters for the SnO_2/ZnO cell are somewhat smaller (η=2.38%, V_{oc}=0.507 V, FF=0.459) but the short-circuit current density (10.24 mA cm^{-2}) is slightly higher compared to the SnO_2/MgO cell (10.18 mA cm^{-2}).

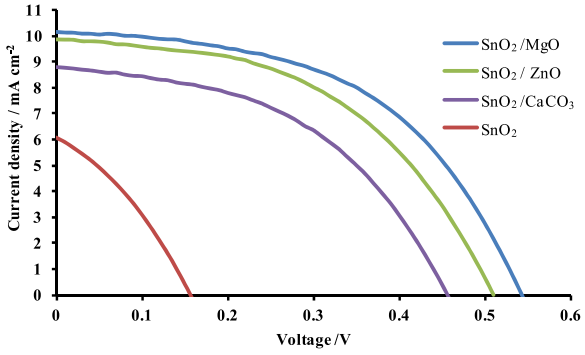

Fig. 4. *IV* curves of different cells.

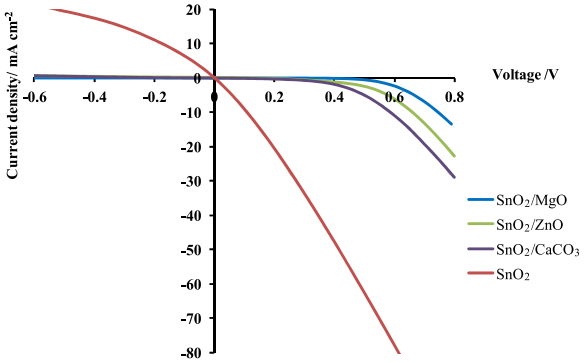

Fig. 5. Dark *IV* curves of different cells.

The dark *IV* curves of the cells are presented in Fig. 5. All the cells with surface passivated SnO_2, shows good rectification. However resistance to electrons entering to TiO_2 is also noticeable as significant forward current appears only at higher voltages. The effect is most pronounced in the MgO system followed by ZnO and CaO. The cell based on pure SnO_2 shows very poor rectification. Compared to electrolytic DSSCs, solid-state versions have much lower efficiencies, an electrolytic DSSC based on SnO_2/MgO gives an efficiency of ~7% [19]. As electrolytic cells have superior dark current rectification, it appears that interfaces in the soild-state cell are more susceptible recombination.

The impedance spectra of the cells under dark conditions, at a bias potential of −0.5 V and the equivalent circuit used for the analysis of the spectra are shown in Fig. 6. The circuit parameters marked in the equivalent circuit are, R_{CE}=resistance at the counter electrode, R_t=transport resistance in the n-type semiconductor, R_{hole}=transport resistance in the p-type semiconductor, R_r=recombination resistance at the p-type semiconductor/n-type semiconductor interface, R_{BL}=resistance at the blocking layer/hole conductor interface, C_μ=capacitance at the p-type semiconductor/n-type semiconductor interface, τ=relaxation time. The values of the parameters R_{CE}, R_t, R_r, R_{hole}, C_μ and τ derived from the analysis are given in Table 5.

Impedance measurements clearly indicates that the presence of

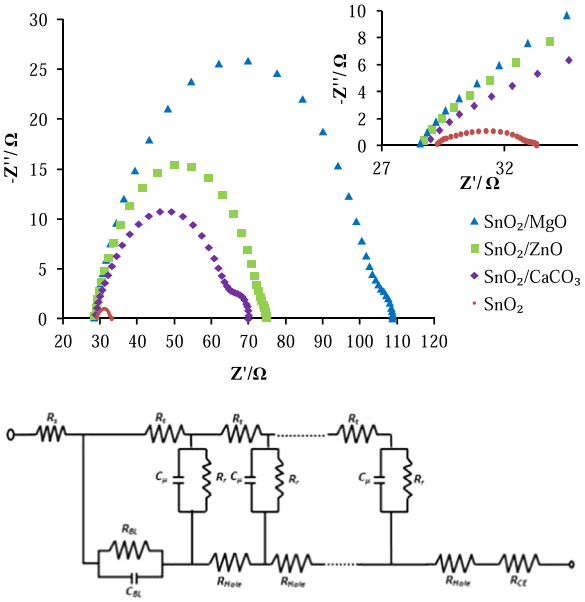

Fig. 6. (a) Impedance spectra of different cells. (b) Equivalent circuit adopted for impedance analysis.

Table 5
Impedance parameters of different cells.

Working electrode	R_{CE}/Ω	R_t/Ω	R_{hole}/Ω	$C_\mu/\mu F$	R_r/Ω	τ/ms
SnO_2	0.7	3.0	0.5	14.7	3.4	0.05
SnO_2/MgO	1.0	21.0	7.0	2.4	74.1	0.18
SnO_2/ZnO	1.0	18.0	4.0	1.6	44.6	0.07
SnO_2/$CaCO_3$	1.0	21.0	7.0	3.0	36.6	0.11

the passivating layer greatly increases the recombination resistance (R_r) by more than one order of magnitude. (Table 5) Recombination resistance increases with the thickness of the passivating film and also depends on the nature of the passivating material. The data presented in Table 5 corresponds to optimum surface concentration of the passivating agent. The effect is most conspicuously evident in SnO_2/MgO system, where $R_r = 74.1\ \Omega$ compared to $3.4\ \Omega$ for SnO_2. It is important to note that this high value of R_r for MgO is the lowest surface concentration (i.e. 8×10^{-9} g cm^{-2} compared to 2.8×10^{-8}, 1.4×10^{-8} g cm^{-2} for ZnO and CaO respectively). Electron transport resistance (R_t) include series resistance contributions from SnO_2 passivating layer and crystallite interconnections and contact at the blocking layer. High values of R_t and R_{hole} for MgO are detrimental to the performance of the cell. An ideal passivating layers would not exhibit the bulk properties of MgO, ZnO or CaO. Presumably, because of unavoidable practical constraints, materials in bulk form may accumulate the SnO_2 matrix. The high capacitance C_μ of SnO_2 of bare SnO_2 films could be understood as a result of a high population of trapping sites that are effectively closed by the passivating agent. MgO in bulk form is highly insulating, this factor may contribute to the high value of R_r for the MgO system. However, we are not in position to provide an unequivocal explanation, as trace amounts of MgO on SnO_2 surface may not have properties similar to bulk MgO Naturally, presence of passivating layers increase the film resistance, but when heterojunction perform as a solar cell, the electron motion through the nanocrystalline matrix is diffusive. In diffusive transport, any modification of the intercrystallites necks could adversely affect the electron diffusion coefficient in contrast to favorable effect of the outer passivating layer. Any signs modification of the crystallite necks due the passivating agent are not discernable SEM examination. Although, conformal coating of passivating layers are expected to avoid modification of the necks, all methods we have adopted to paint layers of MgO, ZnO or CaO after fabrication of the SnO_2 film, failed to yield superior or even comparable results. Immersion of SnO_2 films in precursor solutions containing Mg, Zn or Ca and sintering did not result coating of uniform layers over the SnO_2 crystallites.Passivating layers have reduced the capacitance C_μ by nearly an order of magnitude (2.4, 1.6, and $3.0C_\mu$ μF respectively for SnO_2/MgO, SnO_2/ZnO, SnO_2/CaO respectively, compared to 14.7 C_μ μF for SnO_2). Passivating layers also shift the flat-band level (FBL) of SnO_2 upwards with respect to vacuum zero level [32,33]. Extensive measurements have been conducted to determine the variation of FBL of MgO with the surface concentration of MgO [32]. However, it extremely difficult to assign an optimum thickness to the passivating film. Film was not discernable SEM to assign thickness (t), our previous attempts for measurement with TEM was also unsuccessful. Naively, one can assume $t = W/\rho S$, where W = wt. of passivating agent per unit area, ρ = density and S = effective surface area. However, the material of passivating layer is not really MgO, ZnO or CaO and ρ is uncertain. Assuming ρ as respective bulk densities gives subnanometer values for the film thickness. The shift of FBL rapidly increases with the surface coverage of passivating agent, the shift at the surface coverage of MgO corresponding to the optimum efficiency is ~0.2 eV [32]. The observed change in C_μ could be interpreted as a consequence of the shift of the flat-band potential.

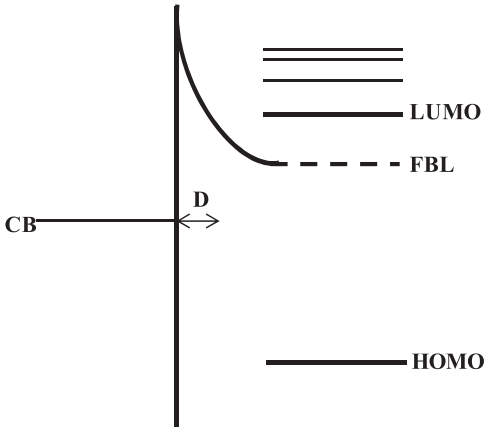

Fig. 7. Schematic energy level diagram of the SnO_2/passivating layer/dye interfaces showing positions of the HOMO, LUMO and vibrational levels of the dye, SnO_2 conduction band (CB), band bending at the passivating layer of thickness D.

It is also seen that the passivating layer increase the relaxation time τ (Table 5) as a natural consequence of the resistance to carrier movement. The effect is strongest in MgO/SnO_2 and least in ZnO/SnO_2 where the relaxation time is comparable to that of the bare SnO_2 system. Although considering bulk properties of the material may not be meaningful, ZnO has very low resistance compared to MgO. An energy level diagram of the SnO_2/passivating layer/dye interfaces showing positions of the HOMO, LUMO and vibrational levels of the dye, SnO_2 conduction band (CB), band bending at the passivating layer of thickness D is represented schematically in Fig. 7. The exact structure of the band profile at the interface could not be ascertained. The sensitivity of the *IV* parameters to the "thickness" of the passivating layer strongly suggests a potential variation at the interface as shown in Fig. 7. Such a profile will sensitively interfere with the carrier injection efficiency, depending on LUMO level of the dye. The photo-excited electron after vibrational relaxation will acquire energy E_{LUMO}, tunnel across the barrier and relax into CB. Tunneling transmission coefficient increases with electron energy and decreases with barrier width D and height. When the tunneled electron relaxes to CB, lowering of energy, greatly reduce backward electron transfer, i.e., geminate recombination is also reduced by the passivating layer. Transient measurements clearly indicate that geminate recombination is faster in dye-sensitized bare SnO_2 compared to TiO_2 [34]. Naturally, barrier also reduces the electron injection rate to some extent. The optimization cell efficiency requires fine tuning of the passivating layer.

4. Conclusions

Other workers have also examined DSSCs with passivating layers of MgO and observed an enhancement of efficiency indicative of recombination suppression and a lowering of the injection efficiency. The reasons for the distinction with the electrolytic version have also been analyzed [4,35]. In the present work DSSC heterostructures of configuration surface passivated SnO_2/indoline dye D149/CuSCN has been extensively examined introducing MgO, ZnO and CaO as the passivating agent and variation of the *IV* parameters with the SnO_2 film thickness is extensively investigated. When the SnO_2 film thickness variation of cell performance was determined, for all thicknesses, the optimum of the short-circuit current and efficiency occurred at a fixed surface concentration of MgO, ZnO and CaO. In all three systems optimum efficiency (2.82%, 2.38%, and 1.84% respectively for SnO_2/

MgO, SnO_2/ZnO, and SnO_2/CaO respectively) occurred at a nearly identical film thickness of 12 μm compared to cells based only of SnO_2, where an optimum efficiency of 0.32% was seen at a film thickness of 9 μm. Compared to previous work [4,35] the dye D149 used here possess very large extinction coefficient, corresponding to a photon mean free path of ~10 μm in the dyed film. The important conclusion of this observation is that, the passivating layers have effectively suppressed the recombination of the electrons as they traverse to the back contact and the film thickness is limited by the photon mean free path (and not the diffusion length). Dark current and impedance measurements also confirm, that recombination is mitigated by the passivating layer. Closure of electron trapping surface states by the passivating agent increase the electron life-time as well the effective electron diffusion coefficient, thereby increasing the electron diffusion length. The passivating layer modulates band profile at the interface shifting the flat-band potential upwards. The modified band structure provides a barrier preventing electron leakage which causes recombination. However, barrier has some detrimental effect on injection efficiency and fine tuning is necessary to achieve best results. The problem seems to be the difficulty of obtaining uniform coverage of requisite surface concentration. Unexpectedly, conformal coatings were found to be inferior to films based on prescriptions, where the passivating agent is introduced to the SnO_2 precursor before film fabrication. Further investigations into film fabrication procedures for incorporation of passivating films and choice other materials would a promising area research for development of efficient DSSSCs and ETA cells.

Acknowledgments

This work was supported by the National Science Foundation of Sri Lanka (NSF/Fellow/2011/02).

References

[1] K. Tennakone, G.R.A. Kumara, A.R. Kumarasinghe, K.G.U. Wijayantha, P. M. Sirimanne, Semicond. Sci. Technol. 10 (1995) 1689–1693, http://dx.doi.org/10.1088/0268-1242/10/12/020.
[2] U. Bach, D. Lupe, P. Comte, J.E. Moser, F. Weissortel, J. Salbeck, H. Spretizer, M. Grätzel, Nature 395 (1998) 583–585.
[3] B. Li, L. Wang, B. Kang, P. Wang, Y. Qiu, Sol. Energy Mater. Sol. Cells 90 (2006) 549–573, http://dx.doi.org/10.1016/j.solmat.2005.04.039.
[4] P. Docampo, S. Guldin, T. Leijtens, N.K. Noel, U. Steiner, H.J. Sanith, Adv. Mater. 26 (2014) 4013–4030, http://dx.doi.org/10.1002/adma.201400486.
[5] B. Xu, E. Sheibani, P. Liu, J. Zhang, H. Tian, N. Vlachopoulos, G. Boschloo, L. Kloo, A. Hagfeldt, L. Sun, Adv. Mater. 26 (2014) 6629–6634, http://dx.doi.org/10.1002/adma.201402415.
[6] K. Tennakone, G.R.A. Kumara, I.R.M. Kottegoda, V.P.S. Perera, G.L.M. Aponsu, J. Phys. D: Appl. Phys. 31 (1998) 2326–2330, http://dx.doi.org/10.1088/0022-3727/31/18/019.
[7] P. Periyat, S.G. Ullattil, Mater. Sci. Semicond. Process. 31 (2015) 139–146, http://dx.doi.org/10.1016/j.mssp.2014.11.022.
[8] R. Konenkamp, L. Dloczik, K. Ernest, C. Olesch, Physica E 14 (2002) 219–223, http://dx.doi.org/10.1016/S1386-9477(02)00387-9.
[9] N.G. Park, Materials Today 18 (2015) 65–72, http://dx.doi.org/10.1016/j.mattod.2014.07.007.
[10] T.T. Bui, F. Goubard, EPJ Photovolt. 4 (2013) 40402–40411 http://dx.doi.org/10.1051/epjpv/2013024.
[11] M. Gratzel, Nature Mater. 13 (2014) 838–842, http://dx.doi.org/10.1038/nmat4065.
[12] Q.B. Meng, K. Takahashi, X.T. Zhang, L. Sutanto, T.N. Rao, O. Sato, A. Fujishima, Langmuir 19 (2003) 3572–3574, http://dx.doi.org/10.1021/la026832n.
[13] K. Tennakone, K.P. Hewaparakkrama, M. Devasurendra, A.H. Jayatissa, Semicond. Sci. Technol. 3 (1988) 382–387, http://dx.doi.org/10.1088/0268-1242/3/4/017.
[14] A. Fujishima, X.T. Zhang, Proc. Jpn. Acad. (2005) 33–42 81 Ser.B.
[15] B.O'. Regan, M. Gratzel, Nature 353 (1991) 737–740, http://dx.doi.org/10.1038/353737a0.
[16] K. Tennakone, G.R.R.A. Kumara, I.R.M. Kottegoda, V.P.S. Perera, Chem. Commun. 1999 (1999) 15–16, http://dx.doi.org/10.1039/A806801A.
[17] E. Guillen, L.M. Peter, J.A. Anta, J. Phys. Chem. C 115 (2011) 22622–22632, http://dx.doi.org/10.1021/jp206698t.
[18] P. Tiwana, P. Docampo, M.B. Johnston, H.J. Snaith, L.M. Herz, ACS Nano 5 (2011) 5158–5166, http://dx.doi.org/10.1021/nn201243y.
[19] K. Tennakone, J. Bandara, P.K.M. Bandaranayake, G.R.A. Kumara, A. Konno, Jpn. J. Appl. Phys. 40 (2001) L732–L734, http://dx.doi.org/10.1143/JJAP.40.L732.
[20] R. Singh, M. Kumar, S. Shankar, R. Singh, A.K. Ghosh, O.P. Thakur, B. Das, Mater. Sci. Semicond. Process. 31 (2015) 310–314, http://dx.doi.org/10.1016/j.mssp.2014.12.010.
[21] C. Prasittichai, J.T. Hupp, J. Phys. Chem. Lett. 1 (2010) 1611, http://dx.doi.org/10.1021/jz100361f.
[22] A.N.M. Green, E. Palomares, S.A. Haque, J.M. Kroon, J. Phys. Chem. B 109 (2005) 12525–12533, http://dx.doi.org/10.1021/jp050145y.
[23] K. Tennakone, V.P.S. Perera, I.R.M. Kottegoda, G. Kumara, J. Phys. D 32 (1999) 374–379, http://dx.doi.org/10.1088/0022-3727/32/4/004.
[24] P. Docampo, P. Tiwana, N. Sakai, H. Mura, L. Herz, T. Murakami, H. Snaith, J. Phys. Chem. C 116 (2012) 22840–22846.
[25] S. Perera, R. Senadeera, K. Tennakone, S. Ito, T. Kitamura, Y. Wada, S. Yanagida, Bull. Chem. Soc. Jpn. 76 (2003) 659–662 , http://dx.doi.org/10.1246/bcsj.76.659.
[26] T. Horiuchi, H. Mura, K. Sumioka, S. Uchida, J. Am. Chem. Soc. 126 (2004) 12218–12219, http://dx.doi.org/10.1021/ja0488277.
[27] G.R.A. Kumara, A. Konno, G.K.R. Senadeera, P.V.V. Jayaweera, D.B.R.A. de Silva, K. Tennakone, Sol. Energy Mater. Sol. Cells 69 (2001) 195–199, http://dx.doi.org/10.1016/S0927-0248(01)00027-7.
[28] E.V.A. Premalal, G.R.R.A. Kumar, R.M.G. Rajapakse, M. Shimomura, K. Murakami, A. Konno, Chem. Commun. 46 (2010) 3360–3362, http://dx.doi.org/10.1039/B927336K.
[29] L. Dloczik, O. Ileperuma, I. Lauermann, L.M. Peter, E.A. Ponomarev, G. Redmond, N.J. Shaw, I. Uhlendorf, J. Phys. Chem. B 49 (1997) 10281–10289, http://dx.doi.org/10.1021/jp972466i.
[30] J. Bisquert, J. Phys. Chem. B108 (2004) 2323–2332, http://dx.doi.org/10.1021/jp035397i.
[31] H.M. Cheng, W.F. Hsieh, Energy Environ. Sci. 3 (2010) 442–447, http://dx.doi.org/10.1039/B915725E.
[32] J. Bandara, U.W. Pradeep, Thin Solid Flims 517 (2008) 952–956, http://dx.doi.org/10.1016/j.tsf.2008.07.031.
[33] J.J. Lee, M.M. Rahman, S. Sarker, N.C.D. Nath, A.J.S. Ahammad, J.K. Lee, Metal oxides and their composites for dye-sensitized solar cells, in: Brahim Attaf (Ed.), Advances in Composite Materials for Medicine and Nanotechnology, Intech, 2011, pp. 181–201, http://dx.doi.org/10.5772/15280.
[34] A.N.M. Green, E. Palomares, S.A. Haque, J.M. Kroon, J.R. Durant, J. Phys. Chem. B 109 (2005) 12525–12533.
[35] P. Docampo, P. Tiwana, N. Sakai, H. Miura, L. Herz, T. Murakami, H.J. Snaith, J. Phys. Chem. C 116 (2012) 22840–22846, http://dx.doi.org/10.1021/jp050145y.